5494 *Biochemistry* **2010,** *49,* 5494–5503
DOI: 10.1021/bi100684g

BIOCHEMISTRY
including biophysical chemistry & molecular biology
Article

Cytidylyl and Uridylyl Cyclase Activity of *Bacillus anthracis* Edema Factor and *Bordetella pertussis* CyaA†

Martin Göttle,[‡] Stefan Dove,[§] Frieder Kees,[‡] Jens Schlossmann,[‡] Jens Geduhn,[∥] Burkhard König,[∥] Yuequan Shen,[⊥] Wei-Jen Tang,[@] Volkhard Kaever,[#] and Roland Seifert*[,#]

[‡]*Department of Pharmacology and Toxicology, and* [§]*Department of Pharmaceutical and Medicinal Chemistry II, Institute of Pharmacy, University of Regensburg, Regensburg, Germany,* [∥]*Institute of Organic Chemistry, University of Regensburg, Regensburg, Germany,* [⊥]*The College of Life Sciences, Nankai University, Tainjin, China,* [@]*Ben May Department for Cancer Research, The University of Chicago, Chicago, Illinois 60637-1546, and* [#]*Institute of Pharmacology, Medical School of Hannover, Hannover, Germany*

Received May 3, 2010; Revised Manuscript Received June 3, 2010

ABSTRACT: Cyclic adenosine 3′,5′-monophosphate (cAMP) and cyclic guanosine 3′,5′-monophosphate (cGMP) are second messengers for numerous mammalian cell functions. The natural occurrence and synthesis of a third cyclic nucleotide (cNMP), cyclic cytidine 3′,5′-monophosphate (cCMP), is a matter of controversy, and almost nothing is known about cyclic uridine 3′,5′-monophosphate (cUMP). *Bacillus anthracis* and *Bordetella pertussis* secrete the adenylyl cyclase (AC) toxins edema factor (EF) and CyaA, respectively, weakening immune responses and facilitating bacterial proliferation. A cell-permeable cCMP analogue inhibits human neutrophil superoxide production. Here, we report that EF and CyaA also possess cytidylyl cyclase (CC) and uridylyl cyclase (UC) activity. CC and UC activity was determined by a radiometric assay, using [α-^{32}P]CTP and [α-^{32}P]UTP as substrates, respectively, and by a high-performance liquid chromatography method. The identity of cNMPs was confirmed by mass spectrometry. On the basis of available crystal structures, we developed a model illustrating conversion of CTP to cCMP by bacterial toxins. In conclusion, we have shown both EF and CyaA have a rather broad substrate specificity and exhibit cytidylyl and uridylyl cyclase activity. Both cCMP and cUMP may contribute to toxin actions.

Cyclic adenosine 3′,5′-monophosphate (cAMP) and cyclic guanosine 3′,5′-monophosphate (cGMP) are second messengers for numerous mammalian cell functions. The natural occurrence of a third cyclic nucleotide (cNMP),[1] cyclic cytidine 3′,5′-monophosphate (cCMP), is a matter of controversy. In 1974, Bloch et al. (*1*) observed that, in contrast to cAMP and cGMP, cCMP initiated the growth of leukemia L-1210 cells. In 1978, Cech and Ignarro (*2*) supposedly identified cCMP formation in mouse liver homogenate, but the methodology was problematic (*3*). The natural occurrence of cCMP in various mammalian organs was later suggested by fast atom bombardment (*4*), but follow-up studies have not yet been performed. A tentative cytidylyl cyclase (CC) activity was reported in various tissues (*2*−*6*), but the molecular identity of the responsible protein has not yet been elucidated. Moreover, cCMP-degrading phosphodiesterase activity was reported (*7*), but again, the identity of the responsible protein is elusive. Furthermore, 10 proteins in brain tissue undergo phosphorylation following stimulation with cCMP (*8*, *9*), but the identity of the responsible protein kinase is unknown. cCMP may also modulate immune system functions. In macrophages, the cell-permeant cCMP analogue dibutyryl-cCMP inhibited thromboxane B_2 and leukotriene B_4 formation (*10*). In human neutrophils, dibutyryl-cCMP inhibited superoxide radical formation and the increase in the cytosolic Ca^{2+} level induced by a chemotactic peptide, resulting in neutrophil inactivation (*11*). Cyclic uridine 3′,5′-monophosphate (cUMP) was thought to occur in mammalian cells as well (*12*), but almost nothing is known about a possible functional role of cUMP.

The causative agents of anthrax disease and whooping cough, *Bacillus anthracis* and *Bodetella pertussis,* respectively, exert their deleterious effects by the release of toxins (*13*, *14*). After interacting with surface receptors of eukaryotic host immune cells and being translocated into the cytosol, the adenylyl cyclase (AC) toxins edema factor (EF) from *B. anthracis* and CyaA from *Bo. pertussis* bind to calmodulin (CaM), resulting in activation of catalysis (*15*, *16*). Both EF and CyaA catalyze massive synthesis of cAMP. Consequently, immune cell function is inhibited, rendering infection more severe (*17*−*19*).

Mammals express nine membranous AC isoforms (mACs 1−9) and a soluble AC. Serendipitously, we discovered 2′(3′)-*O*-(*N*-methylanthraniloyl)-substituted NTPs as competitive inhibitors of mACs and bacterial AC toxins (*20*−*24*). Additionally, PMEApp, the active metabolite of adefovir, a drug for the treatment of chronic hepatitis B virus infection, was identified as a

†Supported by the Deutsche Forschungsgemeinschaft (Graduiertenkolleg 760 "Medicinal Chemistry: Molecular Recognition: Ligand-Receptor Interactions" and Grant Se 529/5-2 to R.S.). This work was supported by the National Institutes of Health (Grant GM 062548 to W.-J.T.).

*To whom correspondence should be addressed: Institute of Pharmacology, Medical School of Hannover, Carl-Neuberg-Str. 1, D-30625 Hannover, Germany. Telephone: +49-511-532-2805. Fax: +49-511-532-4081. E-mail: seifert.roland@mh-hannover.de.

[1]Abbreviations: AC, adenylyl cyclase; CaM, calmodulin; CC, cytidylyl cyclase; cNMP, cyclic nucleoside 3′,5′-monophosphate; EF, edema factor; IC, inosinylyl cyclase; IS, internal standard; LC, liquid chromatography; MANT, methylanthraniloyl; mAC, membranous mammalian AC; NC, nucleotidyl cyclase; NTP, nucleoside 5′-triphosphate; PMEApp, 9-[2-(phosphonomethoxy)ethyl]adenine diphosphate; RT, retention time; sGC, soluble guanylyl cyclase; SPE, solid phase extraction; SRM, selective reaction monitoring; UC, uridylyl cyclase.

 Published on Web 06/03/2010

potent inhibitor of EF and CyaA (*25*). Using crystallographic and molecular modeling approaches, we developed a three-site pharmacophore model for mAC and bacterial AC toxins, with binding domains for the base, the MANT group, and the polyphosphate chain (*23*, *26*). We resolved several EF and CyaA crystal structures and characterized the amino acids important for nucleotide binding and catalysis (*16*, *27*, *28*). Furthermore, we systematically examined the interactions of natural purine and pyrimidine nucleotides and MANT-substituted analogues with EF and CyaA in terms of catalysis, fluorescence changes, and molecular modeling (*26*, *29*). Most surprisingly, MANT-CTP was the most potent competitive EF inhibitor among 16 compounds studied. Taken together, those studies revealed the catalytic sites of EF and CyaA to exhibit conformational flexibility and to accommodate both purine and pyrimidine nucleotides. Those findings also raised the question of whether in addition to ATP, other naturally occurring nucleotides could be toxin substrates.

MATERIALS AND METHODS

Chemicals and Biochemical Reagents. MANT-substituted nucleoside triphosphates (NTPs) of cytidine, inosine, and uridine were synthesized as described previously (*29*). MANT-ATP and MANT-GTP were from Jena Bioscience (Jena, Germany). [α-^{32}P]ATP (800 Ci/mmol), [α-^{32}P]CTP (800 Ci/mmol), and [α-^{32}P]UTP (800 Ci/mmol) were purchased from PerkinElmer (Wellesley, MA). Aluminum oxide N Super 1 was purchased from MP Biomedicals (Eschwege, Germany). Acetonitrile (LC grade), ammonium acetate (p.A.), $CaCl_2$ dihydrate (p.A.), KCl (p.A.), methanol (LC grade), $MnCl_2$ tetrahydrate and $MgCl_2$ hexahydrate (highest quality), *o*-phosphoric acid (p.A.), sodium acetate (p.A.), and triethylamine were from Merck (Darmstadt, Germany). GTP·2Na, ATP·2Na, and cAMP were purchased from Roche (Indianapolis, IN). cCMP·Na, cGMP·Na, cIMP·Na, and cUMP·Na were from Biolog (Bremen, Germany). Bovine serum albumin (fraction V), 2′,3′-cCMP·Na, CMP·2Na, CDP·3Na, CTP·2Na, EGTA, inosine, ITP·3Na, UDP·Na, UMP·Na, and UTP·3Na dihydrate were purchased from Sigma-Aldrich (Seelze, Germany). Tris (ultrapure) was from USB (Cleveland, OH). 9-[2-(Phosphonomethoxy)ethyl]adenine diphosphate (PMEApp) was supplied by Gilead Sciences (Foster City, CA). The full-length AC toxin edema factor (EF) from *B. anthracis* and the catalytic domain of *Bo. pertussis* AC protein (CyaA, amino acids 1−373) were purified as described previously (*15*, *30*). Lyophilized calmodulin (CaM) from bovine brain was purchased from EMD Biosciences, Calbiochem (Darmstadt, Germany).

Isotopic Nucleotidyl Cyclase (*NC*) *Activity Assay*. For the determination of the potency of AC/CC inhibitors, assay tubes contained 10 μL of inhibitor at final concentrations from 1 nM to 100 μM and 20 μL of EF or CyaA dissolved in 75 mM Hepes·NaOH (pH 7.4) supplemented with 0.1% (m/v) bovine serum albumin to prevent protein adsorption. Final protein concentrations were 10 pM EF or CyaA (AC) and 30 pM (CC). Tubes were incubated for 2 min, and reactions were initiated by the addition of 20 μL of reaction mixture consisting of the following components to yield the given final concentrations: 100 mM KCl, 5 mM free Mn^{2+}, 10 μM free Ca^{2+}, 100 μM EGTA, 100 μM cAMP, and 100 nM CaM. In the case of AC activity, ATP was added as the nonlabeled substrate at a final concentration of 40 μM and as radioactive tracer [α-^{32}P]ATP (0.2 μCi/tube). In the case of CC activity, CTP was added as nonlabeled substrate at 10 μM and as radioactive tracer [α-^{32}P]CTP (0.4 μCi/tube). Reactions were conducted for 10 min at 25 °C (AC) and 20 min at 37 °C (CC).

For the determination of K_m and k_{cat} values, assay tubes contained 10 μL of NTP/Mn^{2+} or NTP/Mg^{2+} and 20 μL of reaction mixture as described above. NTP/Mn^{2+} or NTP/Mg^{2+} (1 μM to 2 mM) with 5 mM free Mn^{2+} or Mg^{2+} was added. Reactions were initiated by the addition of 20 μL of EF or CyaA to yield the following final protein concentrations: 10 pM (EF and CyaA AC activities), 40 pM (EF and CyaA CC activities with Mn^{2+}), and 400 pM (EF CC activity with Mg^{2+} and UC activities). The following radioactive tracers remained: [α-^{32}P]ATP (0.2 μCi/tube), [α-^{32}P]CTP (0.8 μCi/tube), and [α-^{32}P]UTP (0.8 μCi/tube). Reactions were conducted for 10 min at 25 °C (AC), 20 min at 37 °C (CC), and 30 min at 37 °C (UC). In saturation experiments using CTP/Mg^{2+} or UTP/Mn^{2+}, no extra nonlabeled cNMPs were added to the reaction mixture. Saturation experiments using CTP/Mn^{2+} were performed in the presence of extra nonlabeled cAMP or cCMP (100 μM each), and in the absence of cNMPs [without yielding significantly different results (data not shown)]. In saturation experiments using ATP/Mg^{2+} or CTP/Mg^{2+} on EF, 10 mM Tris-HCl was included in addition to the reaction mixture, and 1 mM EGTA and 400 nM free Ca^{2+} were used. In those experiments, the reaction mixture was incubated for 5 min at room temperature prior to the addition of CaM and again for 5 min after the addition of CaM to ensure the formation of a steady-state equilibrium of complexing agents and divalent cations. Reactions were terminated by the addition of 20 μL of 2.2 N HCl, and the denaturated protein was sedimented by a 1 min centrifugation at 12000*g*. [^{32}P]cNMP was separated from [α-^{32}P]NTP when the samples were transferred to columns containing 1.4 g of neutral alumina. [^{32}P]cNMP was eluted by the addition of 4 mL of a 0.1 M ammonium acetate solution (pH 7.0) (*31*). Blank values were ∼0.02% of the total amount of [α-^{32}P]NTP added; substrate turnover was <3% of the total added [α-^{32}P]NTP. Samples were filled with 10 mL of Millipore water, and Čerenkov radiation was measured with a PerkinElmer Tricarb 2800TR liquid scintillation analyzer. Free concentrations of divalent cations were calculated with WinMaxC (http://www.stanford.edu/∼cpatton/maxc.html). K_i values, K_m values, and k_{cat} values were calculated using Prism version 4.02 (Graphpad, San Diego, CA).

Nonisotopic NC Assay and HPLC Analysis. In experiments using CyaA, reaction mixtures consisted of the following components and yielded the given final concentrations in a total volume of 3 mL: 1 mM Mn^{2+}, 1 μM Ca^{2+}, 30 mM Hepes·NaOH (pH 7.4), and the corresponding NTP and CaM at concentrations (100 μM) yielding a 1:1 stoichiometry of CaM and bacterial cyclase toxin. In experiments using EF on CTP, UTP, and ITP, reaction mixtures contained 5 mM Mn^{2+} and 5 μM Ca^{2+}. When EF was applied to GTP, the Mn^{2+} concentration was 1 mM and the Ca^{2+} concentration 1 μM. Prior to the addition of the enzyme, two sample aliquots (300 μL each) were taken as negative controls. One sample aliquot was taken and stored on ice; a second sample aliquot lacking enzyme was taken and incubated in parallel with the reaction batch containing enzyme for 60 min at 37 °C. Both negative controls and reaction samples later underwent the sample preparation process described subsequently. Assay tubes were incubated at 37 °C for 4 min, and reactions were initiated by the addition of 300 μL of EF or CyaA. Final protein concentrations ranged between 20 nM bacterial cyclase toxin and 20 nM CaM up to 1500 nM bacterial cyclase toxin and 1500 nM CaM as described in detail in Results. Samples were taken at

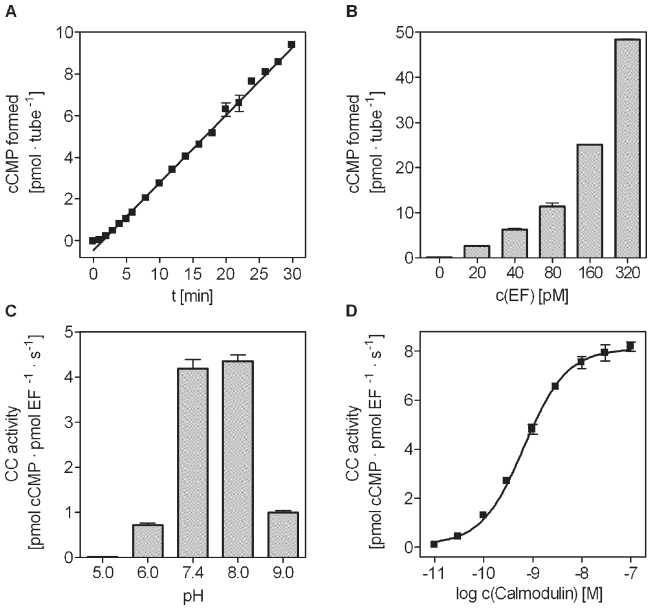

FIGURE 1: Signals obtained using the isotopic EF cytidylyl cyclase activity assay. Reactions were conducted for 20 min at 37 °C as described in Materials and Methods. (A) Time course experiment using 20 pM EF. Reaction mixtures contained the following components to yield the given final concentrations: 100 mM KCl, 5 mM Mn^{2+}, 10 μM free Ca^{2+}, 100 μM EGTA, 10 μM CTP, 0.4 μCi of [α-^{32}P]CTP/tube, and 100 nM CaM. (B) Signal dependence on EF protein concentration. Reaction mixtures contained EF at various concentrations, the components listed for panel A, and additionally 100 μM cAMP. (C) Dependence of CC activity on pH. Reaction mixtures contained 80 pM EF and the components listed for panel B. Buffering systems were 30 mM sodium acetate·HCl (pH 5.0 and 6.0), 30 mM Hepes·NaOH (pH 7.4), and 30 mM Tris·HCl (pH 8.0 and 9.0). (D) Activation of CC activity by CaM. Reaction mixtures contained 5 mM Mn^{2+}, 10 μM free Ca^{2+}, 100 μM EGTA, 10 μM CTP, 0.4 μCi of [α-^{32}P]CTP/tube, 40 pM EF, and CaM at various concentrations. Data shown are means ± the standard deviation of representative experiments performed in duplicate; similar results were obtained in at least three independent experiments.

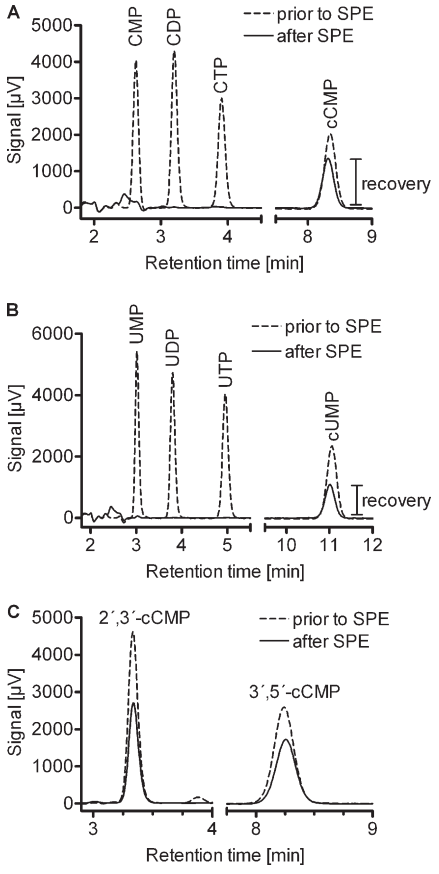

FIGURE 2: HPLC chromatograms of nucleotide mixtures and eluates from solid phase extraction (SPE) using alumina. SPE and HPLC analytics were performed as described in Materials and Methods. (A) Chromatogram of a mixture of 15 μM CMP, CDP, CTP, and 3′,5′-cCMP prior to SPE (---) and chromatogram after SPE (—). (B) Chromatogram of a mixture of 15 μM UMP, UDP, UTP, and 3′,5′-cUMP prior to SPE (---) and chromatogram after SPE (—). (C) Chromatograms of 15 μM 2′,3′-cCMP and 3′,5′-cCMP prior to SPE (---) and chromatogram after SPE (—). The same results were obtained in at least three independent experiments.

reaction times between 1 and 60 min. To achieve protein denaturation, we added sample aliquots (300 μL each) to 600 μL of acetonitrile and cooled them to 4 °C. Three hundred microliters of 40 μM inosine was added as an internal standard (IS). Denatured protein was sedimented by a 1 min centrifugation at 12000*g*. To achieve separation of the aqueous phase from the organic phase, samples were transferred into 5 mL vials and 2 mL of dichloromethane was added. Samples were agitated for 20 min at 4 °C and centrifuged for 5 min at 1000*g*. The aqueous phase was transferred into 1.5 mL vials and stored at −80 °C. Nucleotides were quantified using a Shimadzu LC10 HPLC system with the photometric detector set at 260 nm. A Phenomenex Synergi Fusion-RP HPLC column (150 mm × 4.6 mm, 4 μm particle size, Phenomenex, Aschaffenburg, Germany) was eluted at 1 mL/min with a mobile phase consisting of 100 mM triethylamine with the pH set to 6.6 using *o*-phosphoric acid. The mobile phase contained methanol at a concentration of 6% (v/v) in the case of cCMP, cUMP, or cIMP, 9% (v/v) in the case of cGMP, and 12% (v/v) in the case of cAMP. The mobile phase was run at 1 mL/min, the temperature of the column oven 35 °C, and the injection volume 5 μL. Chromatograms were evaluated using external standardization and Shimadzu LC solution 1.22 SP1.

Mass Spectrometry. LC−MS/MS was performed using an Agilent 1100 HPLC system and a TSQ-7000 Thermoquest Finnigan triple-quadrupole mass spectrometer. A Phenomenex Luna C18 Aqua HPLC column (150 mm × 2 mm, 3 μm particle size) was eluted with the mobile phase at 0.3 mL/min using the following gradient of 0.1% formic acid (A) and acetonitrile (B): 0% B (v/v, from 0 to 2 min), 80% B (v/v, from 2 to 15 min), 80% B (v/v, from 15 to 20 min), 0% B (v/v, from 20 to 25 min), and 0% B (v/v, from 25 to 35 min). The autosampler system was cooled to 5 °C, the temperature of the column oven 40 °C, and the injection volume 20 μL. Upon ESI (capillary temperature of 250 °C, ESI spray voltage of 4 kV), argon was used for collision-induced dissociation with collision energies of 25 V (cCMP), 15 V (cUMP), and 20 V (cIMP). Selective reaction monitoring (SRM) in positive mode was performed by monitoring *m*/*z* 306.0 to 112.2 (cCMP), *m*/*z* 324.2 to 307.0 (cUMP), and *m*/*z* 330.9 to 137.2 (cIMP) transitions. Data were interpreted using Xcalibur version 3.1.

Models of EF and CyaA in Complex with ATP and CTP. The models are based on the crystal structures of EF in complex with 3′-deoxy-ATP [Protein Data Bank (PDB) entry 1xfv (*28*)] and CyaA in complex with PMEApp [PDB entry 1zot (*16*)]. Docking studies were performed with the molecular modeling suite SYBYL version 7.3 (Tripos, LP, St. Louis, MO) on a Silicon Graphics Octane workstation. ATP and CTP were manually docked to both enzymes in a conformation similar to that of 3′-deoxy-ATP bound to EF. Hydrogens were added to the proteins and the water molecules, and the complexes were provided with

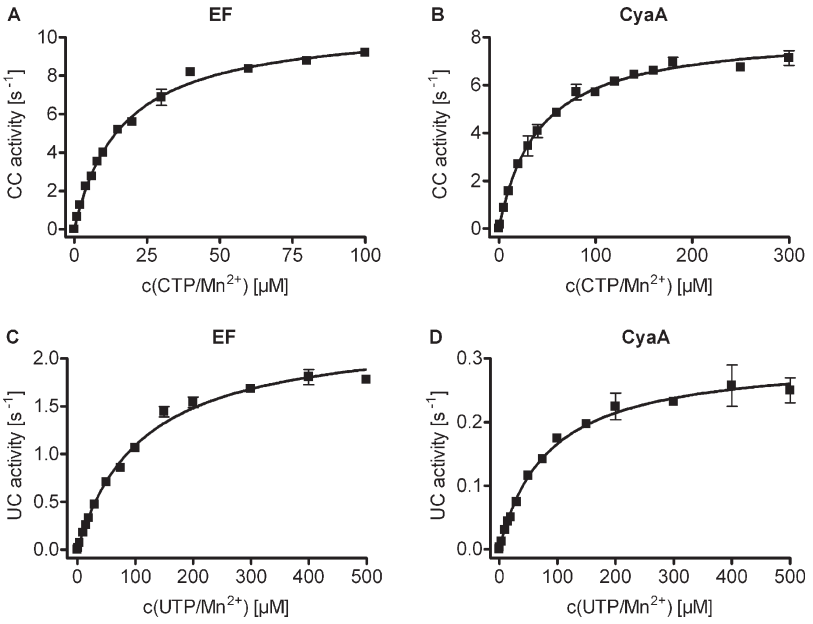

FIGURE 3: Michaelis−Menten kinetics of CC and UC activity of EF and CyaA using the isotopic NC activity. Reactions were conducted as described in Materials and Methods. Reaction mixtures contained the following components to yield the given final concentrations: 100 mM KCl, 10 μM free Ca^{2+}, 100 μM EGTA, 0.8 μCi of [α-^{32}P]CTP/tube or 0.8 μCi of [α-^{32}P]UTP/tube, 100 nM CaM, and nonlabeled cyclic nucleotides as described in Materials and Methods. CTP/Mn^{2+} or UTP/Mn^{2+} (1 μM to 1 mM) with 5 mM free Mn^{2+} was added. The final protein concentration was 40 pM EF or CyaA in the case of CC activity (A and B) and 400 pM EF or CyaA in the case of UC activity (C and D). Reactions were conducted at 37 °C for 20 min in the case of CC activity and for 30 min in the case of UC activity. Data shown are means ± the standard deviation of representative experiments performed in duplicate; similar results were obtained in at least five independent experiments.

Table 1: Kinetic Properties, AC Activities, CC Activities, and UC Activities of EF and CyaA[a]

enzyme	NC activity	cation	K_m (μM)	k_{cat} (s^{-1})	$k_{cat}K_m^{-1}$ (M^{-1} s^{-1})
EF	AC	Mn^{2+}	35.3 ± 3.7	501.5 ± 55.9	1.42×10^7
		Mg^{2+}	175.8 ± 29.9	684.2 ± 272.5	3.89×10^6
	CC	Mn^{2+}	12.5 ± 3.4	8.8 ± 1.4	7.04×10^5
		Mg^{2+}	419.7 ± 115.1	7.2 ± 3.1	1.72×10^4
	UC	Mn^{2+}	134.5 ± 23.5	2.3 ± 0.2	1.71×10^4
CyaA	AC	Mn^{2+}	57.7 ± 4.6	332.0 ± 42.4	5.75×10^6
	CC	Mn^{2+}	46.6 ± 9.7	8.9 ± 2.0	1.91×10^5
	UC	Mn^{2+}	68.6 ± 9.8	0.3 ± 0.05	4.37×10^3

[a]AC activities, CC activities, and UC activities were determined as described in Materials and Methods. NTP/Mn^{2+} or NTP/Mg^{2+} (1 μM to 2 mM) was added, with 5 mM free Mn^{2+} or Mg^{2+}. As a radioactive tracer, [α-^{32}P]-ATP (0.2 μCi/tube), [α-^{32}P]CTP (0.8 μCi/tube), or [α-^{32}P]UTP (0.8 μCi/tube) was added. The final enzyme concentrations were 10 pM (EF and CyaA AC activities), 40 pM (EF and CyaA CC activities with Mn^{2+}), and 400 pM (EF CC activity with Mg^{2+} and UC activities). Reactions were conducted for 10 min at 25 °C (AC), 20 min at 37 °C (CC), and 30 min at 37 °C (UC). Apparent K_m and k_{cat} values were obtained by nonlinear regression analysis of substrate saturation experiments and are means ± the standard deviation of three or four independent experiments performed in duplicate. Saturation curves were analyzed by nonlinear regression using Prism version 4.02 (Graphpad, San Diego, CA).

AMBER_FF99 charges. The models were refined with the AMBER_FF99 force field (*32*) (distance-dependent dielectric constant $\varepsilon = 4$, 25 cycles steepest descent, followed by Powell conjugate gradient, end gradients of 0.01 kcal mol^{-1} $Å^{-1}$).

RESULTS

Isotopic NC Activity Assay. Incubation of 20 pM EF with 0.4 μCi of [α-^{32}P]CTP/tube and 10 μM unlabeled CTP in the presence of 5 mM Mn^{2+} followed by alumina solid phase extraction and liquid scintillation analysis resulted in a pronounced signal increasing in magnitude linearly over time (Figure 1A). Blank values were generally < 0.02% of the total added amount of [α-^{32}P]CTP, indicating full retention of [α-^{32}P]CTP on the column matrix during extraction. With an increase in the enzyme concentration, the magnitude of the resulting signal increased proportionally (Figure 1B). As shown in Figure 1C, the signal intensity showed considerable dependence on pH, with the highest intensity obtained at physiological pH values and poor intensities at low pH values (pH 6.0) or high pH values (pH 9.0). At pH 5.0, no conversion of [α-^{32}P]CTP took place. CaM activated cCMP formation with EC_{50} values of 670 ± 50 pM in the case of EF (Figure 1D) and 80 ± 5 pM in the case of CyaA (data not shown). In the absence of CaM, 40 pM EF increased the magnitude of the signal 3-fold compared with blank values. Similar results were obtained with CyaA (data not shown).

Solid Phase Extraction of cCMP and cUMP and HPLC Analysis. To ensure complete retention of the starting material [α-^{32}P]NTP on alumina columns during solid phase extraction and to determine recovery values for [^{32}P]cNMP, we subjected mixtures of nonlabeled nucleotides to solid phase extraction (SPE) and HPLC analysis. Prior to SPE, HPLC chromatograms from nucleotide mixtures show peaks from 15 μM CMP, CDP, CTP, and 3′,5′-cCMP (Figure 2A, dashed line) as well as from 15 μM UMP, UDP, UTP, and 3′,5′-cUMP (Figure 2B, dashed line). After SPE, 3′,5′-cCMP and 3′,5′-cUMP were eluted while the signals from acyclic nucleotides were missing. The recovery values were 70% in the case of 3′,5′-cCMP and 50% in the case of 3′,5′-cUMP. Therefore, the SPE procedure used in this work completely retained acyclic nucleotides on the alumina columns while cyclic pyrimidine nucleotides were eluted. Thus, the signals detected by liquid scintillation in the isotopic NC assay can result only from cNMPs; nonspecific signals from acyclic nucleotides can be excluded.

Table 2: Inhibitor Potencies at EF and CyaA AC and CC Activities[a]

	K_i (μM)			
nucleotide	EF AC activity	EF CC activity	CyaA AC activity	CyaA CC activity
MANT-ATP	0.43 ± 0.02	0.58 ± 0.03	4.3 ± 0.4[c]	4.4 ± 0.1
MANT-CTP	0.06 ± 0.01[b]	0.08 ± 0.01	1.1 ± 0.1[c]	1.3 ± 0.1
MANT-GTP	2.5 ± 0.1[b]	2.8 ± 0.4	5.9 ± 1.0[c]	6.1 ± 2.0
MANT-ITP	4.1 ± 0.1[b]	5.7 ± 0.03	0.6 ± 0.1[c]	1.0 ± 0.04
MANT-UTP	3.7 ± 0.1[b]	3.8 ± 0.6	2.6 ± 0.3[c]	1.8 ± 0.3

[a]CC activities were determined as described in Materials and Methods. Reaction mixtures contained the following components to yield the given final concentrations: 100 mM KCl, 5 mM free Mn^{2+}, 10 μM free Ca^{2+}, 100 μM EGTA, 10 μM CTP, [α-^{32}P]CTP (0.4 μCi/tube), 100 μM cAMP, and 100 nM CaM. The final protein concentration was 30 pM EF or CyaA, and reactions were conducted for 20 min at 37 °C. K_i values represent the means ± the standard deviation of at least three independent experiments performed in duplicate. Inhibition curves were analyzed by nonlinear regression using Prism version 4.02. [b]From ref *29*. [c]From ref *26*.

To ensure that the cNMPs formed enzymatically were of 3′,5′-cNMP structure and not of the also naturally occurring 2′,3′-cNMP structure, we subjected 15 μM 3′,5′-cCMP and 2′,3′-cCMP to SPE and HPLC analysis. As shown in Figure 2C, a peak from 2′,3′-cCMP at a retention time of 3.3 min was detected, while the retention time of 3′,5′-cCMP was 8.2 min. Both nucleotides were eluted in SPE with recoveries of ~70%. Therefore, 3′,5′-cNMP and 2′,3′-cNMP isomers could easily be discriminated on the basis of their retention times, and cNMPs with 2′,3′-cNMP structure were never detected in enzymatic reactions within this project.

Enzyme Kinetics. Figure 3 shows the results of substrate saturation experiments using the isotopic NC activity assay with CTP/Mn^{2+} or UTP/Mn^{2+} on EF or CyaA; an overview of the kinetic properties of the AC activities, CC activities, and UC activities of EF and CyaA is given in Table 1. Using Mn^{2+}, the K_m value of EF CC activity was 3-fold lower than the K_m value of EF AC activity. The K_m value of EF UC activity was 4-fold higher than the value of AC activity. Using Mg^{2+}, the K_m value of EF CC activity was 2-fold higher than the value of AC activity. Using CyaA and Mn^{2+} yielded similar K_m values in the case of AC, CC, and UC activity. Enzyme activities decreased in the following order: AC > CC > UC (k_{cat} values). Various free Ca^{2+} concentrations between 100 nM and 100 μM did not change this substrate specificity (data not shown). It should also be noted that we determined the AC activity on one hand and CC and UC activities on the other hand at different temperatures (see Materials and Methods), introducing some bias into the interpretation of data. However, these different experimental conditions were necessary to avoid substrate depletion with ATP as the substrate and ensure sufficiently sensitive detection of product formation with CTP and UTP. Using Mn^{2+}, the k_{cat} value of EF CC activity was 57-fold lower than the value of AC activity, and UC activity was even 4-fold lower than CC activity. Using CyaA and Mn^{2+}, the k_{cat} value of CC activity was 37-fold lower than the value of AC activity, and UC activity was even 30-fold lower than CC activity. However, the isotopic assay was sufficiently sensitive to detect even those low enzyme activities. Table 1 also shows the different catalytic efficiencies of EF and CyaA NC reactions given as $k_{cat}K_m^{-1}$ (M^{-1} s^{-1}). Using Mn^{2+}, EF CC activity is 20-fold less efficient than EF AC activity and EF UC activity is even ~800-fold less efficient. Using CyaA, similar data were obtained (Table 1).

Inhibition of NC Activity. EF and CyaA CC activity was inhibited using standard AC inhibitors. Using Mn^{2+}, PMEApp (*25*) inhibited EF AC activity with a K_i value of 2.0 ± 0.5 nM, while PMEApp inhibited CC activity with a K_i value of 4.5 ± 0.4 nM.

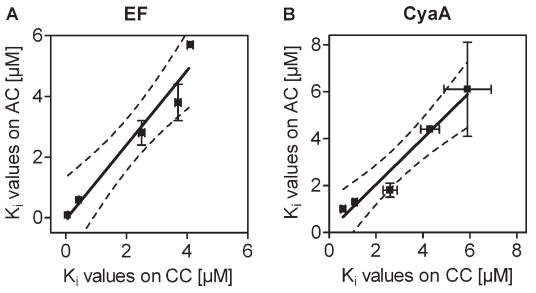

FIGURE 4: Linear correlation of the K_i values of AC and CC inhibition by MANT-nucleotides. Data listed in Table 2 provide the basis for the correlations. Dashed lines represent 95% confidence intervals of the linear regression lines. (A) Inhibition of EF: slope, 1.224 ± 0.1604; r^2, 0.9510; p, 0.0047 (significant). (B) Inhibition of CyaA: slope, 0.9847 ± 0.1226; r^2, 0.9555; p, 0.0040 (significant). Linear regression analysis was performed using Prism version 4.02.

The K_i values of PMEApp on CyaA were 1.0 ± 0.3 nM (AC activity) and 1.1 ± 0.02 nM (CC activity). The K_i values of five MANT-substituted nucleotides on EF and CyaA AC and CC activities are given in Table 2. MANT-CTP was found to be the most potent MANT-nucleotide with respect to EF AC and CC activity, yielding similar K_i values. MANT-ATP inhibited EF CC activity with ~7-fold lower potency than MANT-CTP, followed by MANT-GTP, MANT-UTP, and MANT-ITP. The order of potency of MANT-nucleotides on CyaA CC activity was as follows: MANT-ITP > MANT-CTP > MANT-UTP > MANT-ATP > MANT-GTP. On EF and CyaA, the K_i values of AC and CC inhibition showed significant correlation (Figure 4), indicating that CC and AC activities originated from a single catalytic site.

Nonisotopic NC Assay and HPLC Analysis. EF and CyaA were incubated with several NTPs, and the formation of the corresponding cNMPs was analyzed. Figure 5 shows HPLC chromatograms of reaction samples taken after reaction times between 0 and 60 min. The chromatogram of the incubation of 20 nM EF with 100 μM CTP at a reaction time of 0 min (Figure 5A, purple line) showed a peak resulting from the starting material CTP at a retention time of 3.8 min, while the internal standard (IS) inosine (40 μM) gave a peak at 5.7 min; no additional peaks were detected for the 0 min reaction time at retention times of 6−10 min. With an increasing reaction time, the magnitude of the CTP peak at a retention time of 3.8 min decreased, while at a retention time of 8.3 min, a new peak was detected. The magnitude of this peak increased proportionally with the decrease in the magnitude of the CTP peak. This newly detected signal at a retention time of 8.3 min exhibited a retention time identical to that of 3′,5′-cCMP applied as an external standard (Figure 5A,

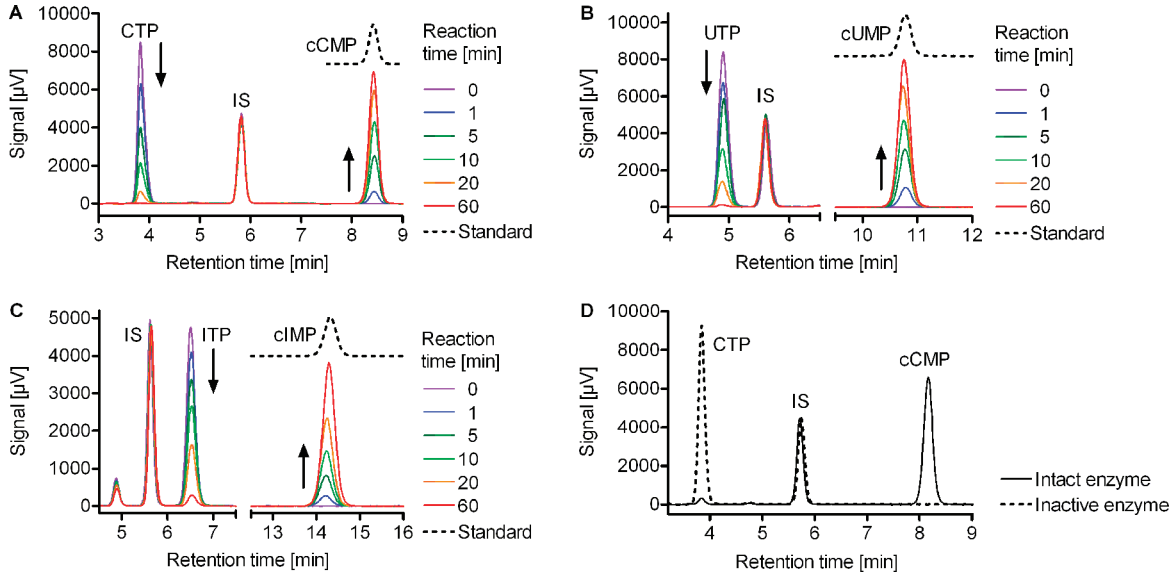

FIGURE 5: HPLC chromatograms of reaction mixtures from the nonisotopic NC assay. The nonisotopic NC assay, sample preparation, and HPLC analytics were conducted as described in Materials and Methods. Reaction mixtures contained 5 mM Mn^{2+}, 5 μM Ca^{2+}, and 100 μM CTP (A), UTP (B), or ITP (C). Protein concentrations were 20 nM EF and 20 nM CaM (A), 120 nM EF and 120 nM CaM (B), and 300 nM EF and 300 nM CaM (C). Samples were withdrawn at the indicated reaction times (colored solid lines). Inosine (20 μM) was added as internal standard (IS); cCMP, cUMP, and cIMP were also added as standard substances (black dotted lines). To prevent the lines from overlapping, the chromatograms of the standard substances were moved vertically. (D) Chromatograms of reaction samples containing 20 nM EF, 20 nM CaM, and 100 μM CTP after a 60 min reaction time. Results for the active enzyme (—) and heat-inactivated enzyme (···). Similar results were obtained in at least three independent experiments.

dashed line). At different reaction times, the internal standard (inosine, 40 μM) yielded constant signals at a retention time of 5.7 min, ensuring reproducible nucleotide recoveries.

To answer the question of which NTP is converted preferentially by EF, ATP, or CTP, both NTPs (100 μM each) were incubated simultaneously with 1 nM EF and 1 nM CaM in one reaction vial, allowing competition of ATP and CTP for the catalytic site. ATP turned out to be converted preferentially; e.g., after incubation for 2 h at 37 °C, the turnover was ~90% for ATP and ~10% for CTP (data not shown). When 120 nM EF was incubated with 100 μM UTP, chromatograms showed the UTP signal at a retention time of 4.9 min (Figure 5B, purple line). With an increasing reaction time, a decrease in the magnitude of the UTP signal was observed, and at a retention time of 10.8 min, a new signal was detected, exhibiting a retention time identical to that of 20 μM 3′,5′-cUMP applied as an external standard (Figure 5B, dashed line). Similarly, upon incubation of 100 μM ITP with 300 nM EF (Figure 5C), a decrease in the magnitude of the ITP peak at a retention time of 6.2 min was observed while the magnitude of a new peak increased at a retention time of 14.2 min, exhibiting a retention time identical to that of 3′,5′-cIMP applied as an external standard (Figure 5C, dashed line).

To ensure that the observed NTP conversions resulted from specific enzymatic activity, 20 nM EF and 100 μM CTP were incubated in a manner similar to the experiment shown in Figure 5A, and for comparison, 20 nM heat-inactivated EF was incubated with 100 μM CTP. After incubation for 60 min using EF, the CTP peak at a retention time of 3.8 min had been converted to a signal at 8.3 min exhibiting the retention time of the cCMP external standard (Figure 5D, solid line). The chromatogram resulting from an incubation for 60 min using heat-inactivated EF showed no new peak from cCMP at a retention time of 8.3 min, but the peak from the starting material CTP persisted at a retention time of 3.8 min (Figure 5D, dashed line). Thus, no conversion of CTP was detected using the heat-inactivated enzyme.

HPLC chromatograms shown in Figure 5 were used to calculate nucleotide concentrations and to depict conversion of NTP to cNMP by EF with an increasing reaction time (Figure 6). EF concentrations were adjusted according to the efficiency of conversion of the individual NTPs. With 20, 120, and 500 nM EF, complete conversion of 100 μM CTP, UTP, and ITP, respectively, occurred within 60 min. When 500 nM EF was incubated with 100 μM GTP, chromatograms showed a decrease in the magnitude of the signal from GTP and a new signal exhibiting the retention time of standard cGMP (data not shown). However, although the EF concentration was high (500 nM), the turnover of GTP within a reaction time of 60 min was only 13%, showing inferior enzymatic activity of EF on GTP as compared to CTP, UTP, and ITP. When CyaA was used instead of EF, similar chromatographic results were obtained (data not shown). Chromatograms also showed complete conversion of CTP, UTP, and ITP within 60 min, yielding peaks at retention times of the corresponding cNMP standards. CyaA concentrations needed for complete turnover of 100 μM NTP within 60 min were 30 nM (CTP), 600 nM (UTP), and 1500 nM (ITP). When 1500 nM CyaA was applied to 100 μM GTP, the turnover within 60 min was 90%.

Mass Spectrometry. To ensure the exact identities of the cNMP products from enzymatic reactions, samples were subjected to LC−MS/MS and the resulting data were compared to results from cNMP standards. Figure 7 shows mass spectra and chromatograms from SRM for cCMP (A−C), cUMP (D−F), and cIMP (G−I). The mass spectrum of cCMP (Figure 7A) shows signals from protonated cCMP (m/z 306.0) and from the protonated cytosine base (m/z 112.2). Selective reaction monitoring of the m/z 306.0 to 112.2 transition proved the existence of cCMP in the nucleotide standard (Figure 7B) as well as in samples from the enzymatic reaction of EF with CTP (Figure 7C). In the case of cUMP, mass signals resulted from the protonated cUMP molecule (m/z 307.0), the cUMP−ammonia adduct (m/z 324.2), and

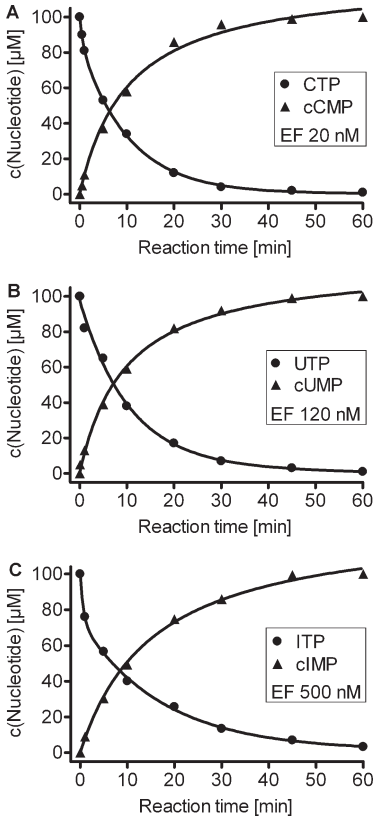

FIGURE 6: Turnover of NTPs to cNMPs by EF using the nonisotopic NC assay. Nucleotide concentrations were calculated by evaluation of the chromatograms shown in Figure 5. CTP (A), UTP (B), or ITP (C), 100 μM each, was converted to the corresponding cyclic nucleotide by the indicated concentrations of EF and equivalent concentrations of CaM ensuring 1:1 EF:CaM stoichiometry. Experiments were performed as described in Materials and Methods. Similar results were obtained in at least three independent experiments.

the protonated uracil base (m/z 113.3) (Figure 7D). SRM of the m/z 324.2 to 307.0 transition proved the existence of cUMP in the nucleotide standard (Figure 7E) and in reaction samples (Figure 7F). The mass spectrum of cIMP (Figure 7G) shows signals from protonated cIMP (m/z 330.9) and from the protonated hypoxanthine base (m/z 137.2). As determined by SRM of the m/z 330.9 to 137.2 transition, cIMP was found in the nucleotide standard and reaction sample (Figure 7H,I).

Modeling of the Nucleotide Binding Modes. The crystal structures of EF in complex with 3′-deoxy-ATP [PDB entry 1xfv (*28*)] and CyaA in complex with PMEApp [PDB entry 1zot (*16*)] were used for docking of ATP and CTP (Figure 8). The nucleotide binding site of EF is a spacious cavity located at the interface of two structural domains, C_A (D294−N349 and A490−K622) and C_B (V350−T489). The position of two Mg^{2+} ions, one coordinated by D491, D493, and H577 and the other by the α-, β-, and γ-phosphates of the substrates, indicates two-metal ion catalysis starting with a nucleophilic attack of the deprotonated 3′-oxygen on the α-phosphorus (*28*). Molecular dynamics simulations suggested that this attack is facilitated by a 3′-endo conformation of the ribosyl moiety, by direct coordination of the 3′-oxygen by the metal, and by the activation of a water molecule by H351 leading to deprotonation of the 3′-OH group (*28*). Figure 8A,B compares the EF binding modes of ATP and CTP. No differences are obvious in the triphosphate or ribosyl regions. The triphosphate groups are cyclically folded due to the coordination by Mg^{2+}. The β- and γ-phosphates form additional salt bridges with K346, K353, and K372. The ribosyl moieties adopt 3′-endo conformations and contact the side chains of L348 and H577. Moreover, electrostatic interactions between the ring oxygens and the amide NH_2 group of N583 are possible. The 3′-oxygen atoms are ~3.4 Å from both Mg^{2+} ions.

The nucleotide bases of ATP and CTP fit to the same pocket mainly consisting of amino acids of EF switch B (G578−N591). The interactions equal those described for the corresponding MANT-ATP and MANT-CTP derivatives (*29*). The amino groups of adenine and cytosine form the same two hydrogen bonds with the backbone oxygens of T548 and T579, and the ring planes are aligned with the side chain of N583. Differences in ATP and CTP binding are not only due to the greater van der Waals surface of ATP (by ~22 Å^2). In the presence of Mn^{2+}, MANT-CTP is ~6 times more potent as an EF inhibitor than its ATP analogue (*29*). A possible reason for the higher affinity may be a water molecule in an ideal position where it forms three hydrogen bonds, bridging the cytosine oxygen with the side chains of R329 and E580 (Figure 8B).

The interactions of ATP and CTP with CyaA are very similar to those with EF. An alignment of the nucleotide binding sites of both enzymes, performed by superposition of the backbone atoms of 15 amino acids surrounding the ligands (root-mean-square distance of 1.22 Å), illustrates the close correspondence (see Figure 8C). Fourteen of the 15 residues are identical; only EF T548 is replaced by CyaA V271. Figure 8D shows the putative interactions of CyaA with CTP. Including the postulated water molecule bridging the cytosine oxygen with the side chains of R41 and E301 and the two hydrogen bonds of the amino group with the backbone oxygens of V271 and T300, all of the CTP−EF interactions are principally reproduced. CyaA H298 adopts a different rotational state compared to EF H377, since the side chain of H398 is not coordinated to a metal ion in the crystal structure, enabling the imidazole NH group to form an additional hydrogen bond with the cytosine oxygen in the minimized model. In the case of CyaA−ATP binding, the complete pattern of EF−ATP interactions can be reproduced (not shown).

DISCUSSION

This study clearly demonstrates that the "AC" toxins EF and CyaA catalyze not only the formation of cAMP but also the formation of cCMP, cUMP, and cIMP. These multiple cNMP-forming enzyme activities originate from a single catalytic site. Considering the previously reported broad base specificities of the two toxins (*21*, *26*, *29*), our data are not totally unexpected. The development of the cCMP field had been seriously hampered by methodological problems (*2*, *3*). In this study, we describe straightforward radiometric and HPLC-based methods for assessing cNMP formation. The sensitive and simple radiometric method described herein can be applied in any biochemical laboratory without specialized equipment. The HPLC method can be used to prepare isotopically labeled cNMPs as standards for mass spectrometry that are not commercially available.

The substrate saturation experiments show some intriguing differences between the results with Mn^{2+} and Mg^{2+}. Generally, the k_{cat} values of EF AC and EF CC activity are similar and rather independent of the cation, but K_m is by a factor of ~5 (AC) and ~34 (CC) lower in the case of Mn^{2+}. Thus, not the enzyme mechanism, but the substrate affinity is mainly affected by the cation species. Additionally, the K_m value of CTP is 3-fold lower than that of ATP with Mn^{2+} but more than 2-fold higher compared to that for ATP with Mg^{2+}. This corresponds to our

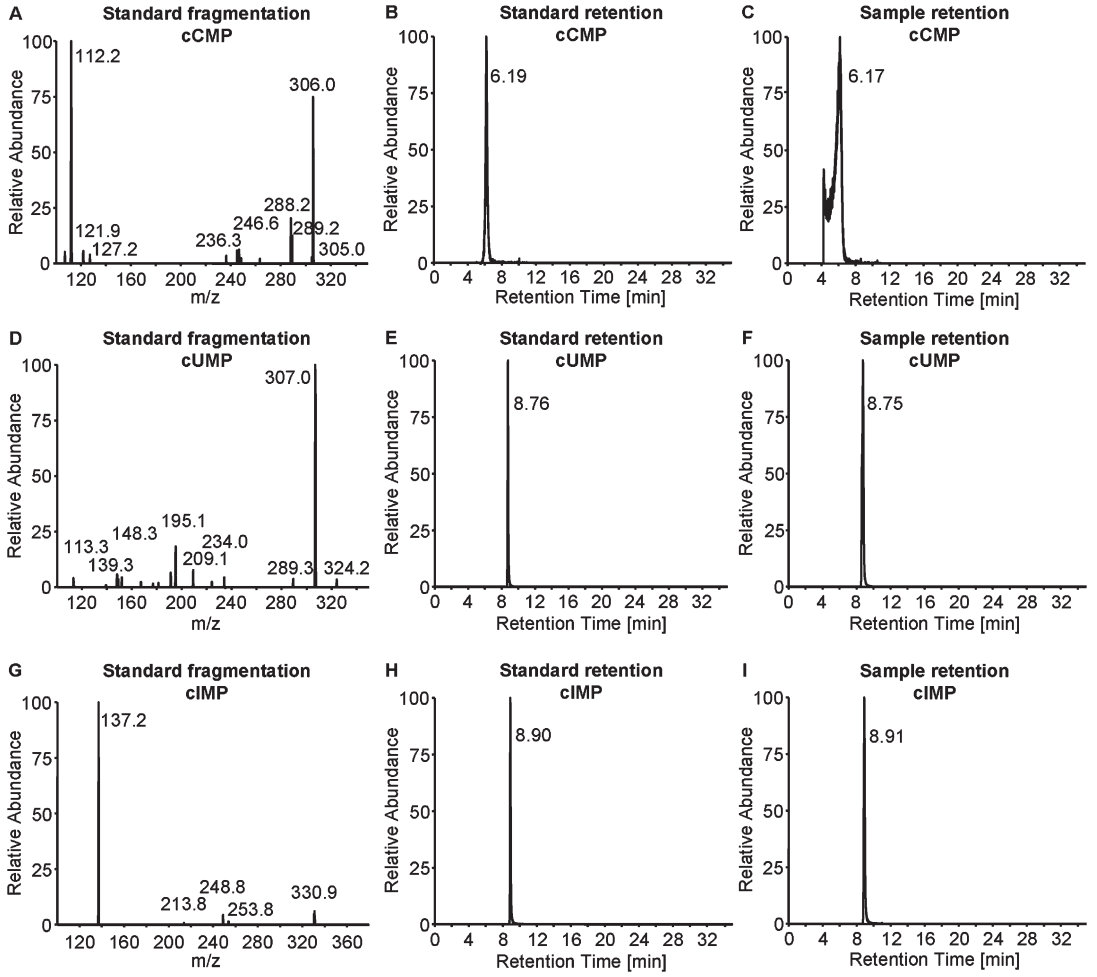

FIGURE 7: Verification of the identities of the cyclic nucleotides formed in the nonisotopic NC assay by mass spectrometry. HPLC-MS analytics were performed as described in Materials and Methods. Shown are fragmentation patterns of the standard cyclic nucleotides, chromatograms from standard cyclic nucleotides, and chromatograms from reaction samples for cCMP (A−C), cUMP (D−F), and cIMP (G−I). Similar results were obtained in at least three independent experiments.

previous findings that the affinities of MANT-CTP for CyaA (*26*) and EF (*29*) were significantly higher than those of MANT-ATP only if Mn^{2+} was used as the divalent cation. These discrepancies are probably not due to different direct interactions of the substrates or the products with the cations since the binding constants of UTP and PP_i for Mg^{2+} and Mn^{2+}, respectively, are very similar (*33*). Therefore, the reasons for the higher nucleotide affinity with Mn^{2+} as a cofactor should rely on interactions within the enzyme−substrate complex. However, if one compares the mean Mg^{2+}−O distances of the structures used for modeling, EF in complex with 3′-deoxy-ATP (2.47 ± 0.22 Å) (*28*) and CyaA in complex with PMEApp (2.30 ± 0.34 Å) (*16*), with the mean Mn^{2+}−O distance (2.53 ± 0.18 Å) in the highest-resolution AC structure with Mn^{2+} [PDB entry 1ybu (*34*)], it becomes obvious that different cation−oxygen distances do not play an essential role. An exchange of the cation species will probably induce subtle rearrangements of the catalytic site in the enzyme−substrate complex that mainly affect the binding affinity of CTP. This "fine-tuning" is not obvious from the crystal structures with limited resolution and can, if at all, only be analyzed by ab initio quantum chemical calculations. Similar differences between Mn^{2+} and Mg^{2+} exist also in the case of mACs (*35*). Compared to Mg^{2+}, Mn^{2+} significantly reduces the K_m value of ATP and increases the inhibitory potency of a substrate analogue but has a weaker influence on V_{max}.

In our previous studies, we characterized the interactions of the catalytic sites of EF and CyaA with various purine and pyrimidine NTPs and MANT-NTPs (*26*, *29*). We developed a three-site pharmacophore model for mAC, EF, and CyaA attributing major importance to the MANT substituent for nucleotide affinity, followed by the phosphate tail (*23*). The higher affinity of MANT-NTPs is a result of additional hydrophobic interactions of the MANT group with F586 in EF and F306 in CyaA (*26*, *29*). The base turned out to play a minor role as the catalytic site of AC is spacious and conformationally flexible and accommodates various purine and pyrimidine nucleotides (*26*, *29*). Using kinetic FRET competition experiments, we have shown that MANT-ATP and MANT-CTP reversibly bind to the catalytic site of EF, further corroborating a single catalytic site in EF (*29*). The binding modes suggested for the bases in MANT-ATP and MANT-CTP are the same as in the case of ATP and CTP, respectively (see Figure 8). The affinity of CTP and MANT-CTP may be especially due to the possibility that a water molecule mediates a network of hydrogen bonds between the cytosine oxygen and the side chains of R329 and E580. Taken together, these results confirm that various bases, in particular adenine and cytosine, can be accommodated by the EF catalytic site. Also in the case of CyaA, modeling of the binding modes of MANT-NTPs indicated that all bases are aligned in similar positions (*26*). ATP, CTP, and their MANT derivatives can form the same interactions with EF

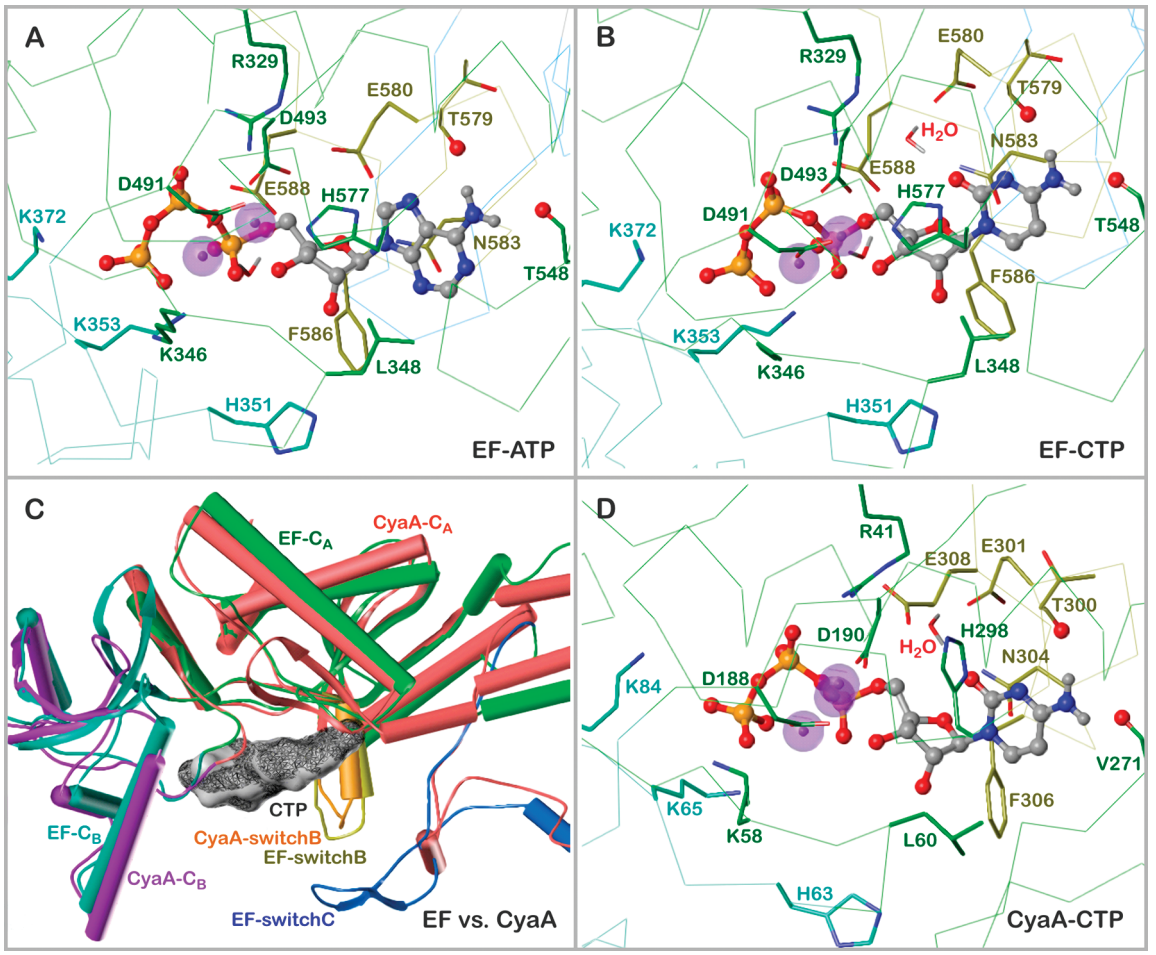

FIGURE 8: Suggested interaction of nucleotides with EF and CyaA. The minimized models are based on the crystal structures of EF in complex with 3′-deoxy-ATP (*28*) and CyaA in complex with PMEApp (*16*). Colors of atoms, unless otherwise indicated: orange for P, red for O, blue for N, gray for C and H, and purple spheres for Mg^{2+}. (A) Interaction of EF with ATP. (B) Interaction of EF with CTP. (C) Alignment of the nucleotide binding sites of EF and CyaA in complex with CTP [represented as MOLCAD surfaces, bound to EF (black lines) and bound to CyaA (gray opaque)]. Enzyme models: cylinders for helices, ribbons for β-sheets, tubes for loops, EF domain C_A colored green, domain C_B colored green-blue, switch B colored yellow, switch C colored blue, CyaA domain C_A colored pink, domain B colored purple, and switch C_B colored orange. (D) Interaction of CTP with CyaA. In panels A, B, and D, the side chains of the amino acids of the binding sites are drawn as sticks and labeled. Colors of C atoms and Cα traces: domain A in green, domain B in green-blue, and switch B in yellow. The backbone oxygen atoms suggested to form hydrogen bonds with the amino groups of ATP and CTP are marked as spheres.

and CyaA. However, the K_m value of UTP for EF is 4-fold higher than that of ATP, whereas the affinities of the purines MANT-GTP and MANT-ATP as well as of the pyrimidines MANT-UTP, MANT-ITP, and MANT-CTP for CyaA are similar. A possible reason is that EF D582 corresponds to CyaA N303. After a slight change of the rotamer state of the asparagine side chain, the amide may serve as a hydrogen donor for the carbonyl oxygens in the purine 6 and pyrimidine 4 positions. Collectively, our studies demonstrate the broad base specificity of the catalytic sites of EF and CyaA in terms of both substrates and inhibitors.

Our data on CC and UC activities of bacterial toxins have important implications for the cNMP field in general. Considering the fact that bacterial AC toxins, mACs, and sGC all exhibit broad base specificity (*21*−*24*, *36*), the question of whether mammalian NCs synthesize cCMP and cUMP as well arises. The analysis of this issue is not trivial since the catalytic activities of mammalian NCs are much lower than those of bacterial toxins. Hence, the sensitivity of the radiometric method described in this report may not be sufficient for the detection of such activities. To improve sensitivity, we are currently developing highly sensitive mass spectrometry methods for quantitative detection of cNMPs. To this end, we have studied whether sGC and mACs exhibit UC activity using the radiometric approach. In fact, sGC exhibits nitric oxide-stimulated UC activity, whereas for recombinant mACs 2 and 5 expressed in Sf9 insect cell membranes, no UC activity was detected (*21*). This is quite remarkable since the affinity of all these NCs for inhibitory UTP and CTP analogues is quite similar (*36*). These data are a first indication that CC and UC activities of bacterial and mammalian NCs do not simply represent "substrate leakiness" but reflect poorly understood functional differences between the various cNMPs. Almost nothing is known about a possible functional role of cUMP. As the cell-permeant cCMP analogue dibutyryl-cCMP blunts host immune responses (*10*, *11*), we hypothesize that the formation of cCMP by EF and CyaA synergizes with cAMP to disrupt immune responses. Finally, our data urgently call for an in-depth analysis of the substrate specificity of mammalian NCs with the methods described in this report or even more sensitive mass spectrometry methods.

ACKNOWLEDGMENT

We thank Mrs. Susanne Brüggemann, Mr. Josef Kiermeier, and Mrs. Astrid Seefeld for expert technical assistance. Thanks are also due to the reviewers for their constructive critique.

REFERENCES

1. Bloch, A., Dutschman, G., and Maue, R. (1974) Cytidine 3′,5′-monophosphate (cyclic CMP). II. Initiation of leukemia L-1210 cell growth *in vitro*. *Biochem. Biophys. Res. Commun. 59*, 955–959.
2. Cech, S. Y., and Ignarro, L. J. (1978) Cytidine 3′,5′-monophosphate (cyclic CMP) formation by homogenates of mouse liver. *Biochem. Biophys. Res. Commun. 80*, 119–125.
3. Gaion, R. M., and Krishna, G. (1979) Cytidylate cyclase: The product isolated by the method of Cech and Ignarro is not cytidine 3′,5′-monophosphate. *Biochem. Biophys. Res. Commun. 86*, 105–111.
4. Newton, R. P., Salih, S. G., Salvage, B. J., and Kingston, E. E. (1984) Extraction, purification and identification of cytidine 3′,5′-cyclic monophosphate from rat tissues. *Biochem. J. 221*, 665–673.
5. Newton, R. P., Salvage, B. J., and Hakeem, N. A. (1990) Cytidylate cyclase: Development of assay and determination of kinetic properties of a cytidine 3′,5′-cyclic monophosphate-synthesizing enzyme. *Biochem. J. 265*, 581–586.
6. Newton, R. P., Groot, N., van Geyschem, J., Diffley, P. E., Walton, T. J., Bayliss, M. A., Harris, F. M., Games, D. E., and Brenton, A. G. (1997) Estimation of cytidylyl cyclase activity and monitoring of side-product formation by fast-atom bombardment mass spectrometry. *Rapid Commun. Mass Spectrom. 11*, 189–194.
7. Newton, R. P., Bayliss, M. A., Khan, J. A., Bastani, A., Wilkins, A. C., Games, D. E., Walton, T. J., Brenton, A. G., and Harris, F. M. (1999) Kinetic analysis of cyclic CMP-specific and multifunctional phosphodiesterases by quantitative positive-ion fast-atom bombardment mass spectrometry. *Rapid Commun. Mass Spectrom. 13*, 574–584.
8. Bond, A. E., Dudley, E., Tuytten, R., Lemiere, F., Smith, C. J., Esmans, E. L., and Newton, R. P. (2007) Mass spectrometric identification of rab23 phosphorylation as a response to challenge by cytidine 3′,5′-cyclic monophosphate in mouse brain. *Rapid Commun. Mass Spectrom. 21*, 2685–2692.
9. Ding, S., Bond, A. E., Lemiere, F., Tuytten, R., Esmans, E. L., Brenton, A. G., Dudley, E., and Newton, R. P. (2008) Online immobilized metal affinity chromatography/mass spectrometric analysis of changes elicited by cCMP in the murine brain phosphoproteome. *Rapid Commun. Mass Spectrom. 22*, 4129–4138.
10. Elliott, G. R., Lauwen, A. P., and Bonta, I. L. (1991) Dibutyryl cytidine 3′:5′-cyclic monophosphate: An inhibitor of A23187-stimulated macrophage leukotriene B_4 synthesis. *Agents Actions 32*, 90–91.
11. Ervens, J., and Seifert, R. (1991) Differential modulation by N^4,2′-*O*-dibutyryl cytidine 3′:5′-cyclic monophosphate of neutrophil activation. *Biochem. Biophys. Res. Commun. 174*, 258–267.
12. Newton, R. P., Kingston, E. E., Hakeem, N. A., Salih, S. G., Beynon, J. H., and Moyse, C. D. (1986) Extraction, purification, identification and metabolism of 3′,5′-cyclic UMP, 3′,5′-cyclic IMP and 3′,5′-cyclic dTMP from rat tissues. *Biochem. J. 236*, 431–439.
13. Ahuja, N., Kumar, P., and Bhatnagar, R. (2004) The adenylate cyclase toxins. *Crit. Rev. Microbiol. 30*, 187–196.
14. Ladant, D., and Ullmann, A. (1999) *Bordetella pertussis* adenylate cyclase: A toxin with multiple talents. *Trends Microbiol. 7*, 172–176.
15. Drum, C. L., Yan, S. Z., Sarac, R., Mabuchi, Y., Beckingham, K., Bohm., A., Grabarek, Z., and Tang, W. J. (2000) An extended conformation of calmodulin induces interactions between the structural domains of adenylyl cyclase from *Bacillus anthracis* to promote catalysis. *J. Biol. Chem. 275*, 36334–36340.
16. Guo, Q., Shen, Y., Lee, Y. S., Gibbs, C. S., Mrksich, M., and Tang, W. J. (2005) Structural basis for the interaction of *Bordetella pertussis* adenylyl cyclase toxin with calmodulin. *EMBO J. 24*, 3190–3201.
17. Hewlett, E. L., Donato, G. M., and Gray, M. C. (2006) Macrophage cytotoxicity produced by adenylate cyclase toxin from *Bordetella pertussis*: More than just making cyclic AMP!. *Mol. Microbiol. 59*, 447–459.
18. Paccani, S. R., Tonello, F., Ghittoni, R., Natale, M., Muraro, L., D'Elios, M. M., Tang, W. J., Montecucco, C., and Baldari, C. T. (2005) Anthrax toxins suppress T lymphocyte activation by disrupting antigen receptor signalling. *J. Exp. Med. 201*, 325–331.
19. Tournier, J. N., Quesnel-Hellmann, A., Mathieu, J., Montecucco, C., Tang, W. J., Mock, M., Vidal, D. R., and Goossens, P. L. (2005) Anthrax edema toxin cooperates with lethal toxin to impair cytokine secretion during infection of dendritic cells. *J. Immunol. 174*, 4934–4941.
20. Johnson, R. A., and Shoshani, I. (1990) Inhibition of *Bordetella pertussis* and *Bacillus anthracis* adenylyl cyclases by polyadenylate and "P"-site agonists. *J. Biol. Chem. 265*, 19035–19039.
21. Gille, A., Lushington, G. H., Mou, T. C., Doughty, M. B., Johnson, R. A., and Seifert, R. (2004) Differential inhibition of adenylyl cyclase isoforms and soluble guanylyl cyclase by purine and pyrimidine nucleotides. *J. Biol. Chem. 279*, 19955–19969.
22. Mou, T. C., Gille, A., Fancy, D. A., Seifert, R., and Sprang, S. R. (2005) Structural basis for the inhibition of mammalian membrane adenylyl cyclase by 2′(3′)-*O*-(*N*-Methylanthraniloyl)-guanosine 5′-triphosphate. *J. Biol. Chem. 280*, 7253–7261.
23. Mou, T. C., Gille, A., Suryanarayana, S., Richter, M., Seifert, R., and Sprang, S. R. (2006) Broad specificity of mammalian adenylyl cyclase for interaction with 2′,3′-substituted purine- and pyrimidine nucleotide inhibitors. *Mol. Pharmacol. 70*, 878–886.
24. Gille, A., and Seifert, R. (2003) 2′(3′)-*O*-(*N*-methylanthraniloyl)-substituted GTP analogs: A novel class of potent competitive adenylyl cyclase inhibitors. *J. Biol. Chem. 278*, 12672–12679.
25. Shen, Y., Zhukovskaya, N. L., Zimmer, M. I., Soelaiman, S., Bergson, P., Wang, C. R., Gibbs, C. S., and Tang, W. J. (2004) Selective inhibition of anthrax edema factor by adefovir, a drug for chronic hepatitis B virus infection. *Proc. Natl. Acad. Sci. U.S.A. 101*, 3242–3247.
26. Göttle, M., Dove, S., Steindel, P., Shen, Y., Tang, W. J., Geduhn, J., König, B., and Seifert, R. (2007) Molecular analysis of the interaction of *Bordetella pertussis* adenylyl cyclase with fluorescent nucleotides. *Mol. Pharmacol. 72*, 526–535.
27. Drum, C. L., Yan, S. Z., Bard, J., Shen, Y. Q., Lu, D., Soelaiman, S., Grabarek, Z., Bohm, A., and Tang, W. J. (2002) Structural basis for the activation of anthrax adenylyl cyclase exotoxin by calmodulin. *Nature 415*, 396–402.
28. Shen, Y., Zhukovskaya, N. L., Guo, Q., Florian, J., and Tang, W. J. (2005) Calcium-independent calmodulin binding and two-metal-ion catalytic mechanism of anthrax edema factor. *EMBO J. 24*, 929–941.
29. Taha, H. M., Schmidt, J., Göttle, M., Suryanarayana, S., Shen, Y., Tang, W. J., Gille, A., Geduhn, J., König, B., Dove, S., and Seifert, R. (2009) Molecular analysis of the interaction of anthrax adenylyl cyclase toxin, edema factor, with 2′(3′)-*O*-(*N*-(methyl)anthraniloyl)-substituted purine and pyrimidine nucleotides. *Mol. Pharmacol. 75*, 693–703.
30. Drum, C. L., Shen, Y., Rice, P. A., Bohm, A., and Tang, W. J. (2001) Crystallization and preliminary X-ray study of the edema factor exotoxin adenylyl cyclase domain from *Bacillus anthracis* in the presence of its activator, calmodulin. *Acta Crystallogr. D57*, 1881–1884.
31. Alvarez, R., and Daniels, D. V. (1990) A single column method for the assay of adenylate cyclase. *Anal. Biochem. 187*, 98–103.
32. Cornell, W. D., Cieplak, P., Bayly, C. I., Gould, I. R., Merz, K. M. J., Ferguson, D. M., Spellmeyer, D. C., Fox, T., Caldwell, J. W., and Kollman, P. A. (1995) A second generation force field for the simulation of proteins and nucleic acids. *J. Am. Chem. Soc. 117*, 5179–5197.
33. Zea, C. J., Camci-Unal, G., and Pohl, N. L. (2008) Thermodynamics of binding of divalent magnesium and manganese to uridine phosphates: Implications for diabetes-related hypomagnesaemia and carbohydrate biocatalysis. *Chem. Cent. J. 2*, 15.
34. Sinha, S. C., Wetterer, M., Sprang, S. R., Schultz, J. E., and Linder, J. U. (2005) Origin of asymmetry in adenylyl cyclases: Structures of *Mycobacterium tuberculosis* Rv1900c. *EMBO J. 24*, 663–673.
35. Dessauer, C. W., Scully, T. T., and Gilman, A. G. (1997) Interactions of forskolin and ATP with the cytosolic domains of mammalian adenylyl cyclase. *J. Biol. Chem. 272*, 22272–22277.
36. Suryanarayana, S., Göttle, M., Hübner, M., Gille, A., Mou, T.-C., Sprang, S. R., Richter, M., and Seifert, R. (2009) Differential inhibition of various adenylyl cyclase isoforms and soluble guanylyl cyclase by 2′,3′-*O*-(2,4,6-trinitrophenyl)-substituted nucleoside 5′-triphosphates. *J. Pharmacol. Exp. Ther. 330*, 687–695.